Publications of the Astronomical Society of Japan, 2025, **77**(SP1), S270–S275
https://doi.org/10.1093/pasj/psaf089
Advance access publication date: 2025 August 20

XRISM observation of the Ophiuchus galaxy cluster: Quiescent velocity structure in the dynamically disturbed core

Yutaka Fujita,[1,*] Kotaro Fukushima,[2] Kosuke Sato,[3] Yasushi Fukazawa,[4] and Marie Kondo[5]

[1]Department of Physics, Graduate School of Science, Tokyo Metropolitan University, 1-1 Minami-Osawa, Hachioji-shi, Tokyo 192-0397, Japan
[2]Institute of Space and Astronautical Science, JAXA, 3-1-1 Yoshinodai, Chuo-ku, Sagamihara, Kanagawa 252-5210, Japan
[3]Department of Astrophysics and Atmospheric Sciences, Kyoto Sangyo University, Kamigamo-motoyama, Kita-ku, Kyoto, Kyoto 603-8555, Japan
[4]Department of Physical Science, Hiroshima University, 1-3-1 Kagamiyama, Higashi-Hiroshima, Hiroshima 739-8526, Japan
[5]Graduate School of Science and Engineering, Saitama University, 255 Shimo-Ohkubo, Sakura, Saitama, Saitama 338-8570, Japan
*E-mail: y-fujita@tmu.ac.jp

Abstract

We present high-resolution X-ray spectroscopic observations of the Ophiuchus galaxy cluster core using the X-Ray Imaging and Spectroscopy Mission (XRISM) satellite. Despite previous observations revealing multiple cold fronts and dynamical disturbances in the cluster core, our XRISM observations show low gas velocity dispersions of $\sigma_v = 115 \pm 7\,\mathrm{km\,s^{-1}}$ in the inner region ($\lesssim$25 kpc) and $\sigma_v = 186 \pm 9\,\mathrm{km\,s^{-1}}$ in the outer region (∼25–50 kpc). The gas temperatures are $kT = 5.8 \pm 0.2$ and 8.4 ± 0.2 keV for the inner and outer regions, respectively, with metal abundances of $Z = 0.75 \pm 0.03\,Z_\odot$ (inner) and $0.44 \pm 0.02\,Z_\odot$ (outer). The measured velocity dispersions correspond to non-thermal pressure fractions of only $1.4 \pm 0.2\%$ (inner) and $2.5 \pm 0.2\%$ (outer), indicating highly subsonic turbulence. Our analysis of the bulk gas motion indicates that the gas in the inner region is nearly at rest relative to the central galaxy ($|v_{\rm bulk}| = 8 \pm 7\,\mathrm{km\,s^{-1}}$), while the outer region exhibits a moderate motion of $|v_{\rm bulk}| = 104 \pm 7\,\mathrm{km\,s^{-1}}$. Assuming the velocity dispersion arises from turbulent motions, the turbulent heating rate is ∼40% of the radiative cooling rate, although there is some uncertainty. This suggests that the heating and cooling of the gas are not currently balanced. The activity of the central active galactic nucleus has apparently weakened. The sloshing motion that created the cold fronts may now be approaching a turning point at which the velocity is minimum. Alternatively, the central galaxy and the associated hot gas could be moving nearly parallel to the plane of the sky.

Keywords: galaxies: clusters: individual (Ophiuchus) — galaxies: clusters: intracluster medium — galaxies: elliptical and lenticular, cD

1 Introduction

Galaxy clusters are the largest gravitationally bound structures in the Universe, representing the endpoints of cosmic structure formation (Kravtsov & Borgani 2012). These massive systems, with masses ranging from 10^{14} to $10^{15}\,M_\odot$, are dominated by dark matter but contain significant amounts of hot, X-ray emitting gas known as the intracluster medium (ICM). The ICM is heated to temperatures of 10^7–10^8 K through gravitational processes during cluster assembly (Sarazin 1988).

The physics of the ICM is governed by a complex interplay of gravitational heating, radiative cooling, and various feedback mechanisms. In the central regions of many clusters, the ICM exhibits a "cool core" structure characterized by a sharp increase in gas density and decrease in temperature toward the cluster center. These conditions lead to radiative cooling times that are much shorter than the Hubble time, theoretically resulting in massive cooling flows with rates of hundreds to thousands of solar masses per year (Fabian 1994).

However, observations consistently reveal a fundamental discrepancy known as the "cooling flow problem." Despite the short cooling times in cluster cores, line emissions from cooling gas are not observed (Ikebe et al. 1997; Kaastra et al. 2001; Peterson et al. 2001; Tamura et al. 2001). This suggests that some form of heating mechanism must be operating to prevent or significantly reduce the cooling flow.

Active galactic nucleus (AGN) feedback has emerged as the leading solution to the cooling flow problem. The supermassive black holes at the centers of brightest cluster galaxies (BCGs) can inject enormous amounts of energy into the surrounding ICM through relativistic jets and outflows (Churazov et al. 2000; McNamara & Nulsen 2007; Fabian 2012). These AGN-driven processes create X-ray cavities, inflate radio bubbles, and drive shock waves and turbulence throughout the cluster core. The energy deposited by AGN activity appears to be sufficient to offset radiative cooling losses in many systems.

However, the detailed mechanisms by which AGN energy is transferred to the ICM remain poorly understood. The energy must somehow be converted from the highly collimated, relativistic jets into thermal energy that can heat the diffuse gas. Proposed mechanisms include the buoyant rise and mixing of relativistic plasma, cosmic rays, and the dissipation of turbulent motions (Churazov et al. 2001; Hillel & Soker 2017; Fujita & Ohira 2013; Zhuravleva et al. 2014).

Received: 2025 July 1; **Accepted:** 2025 July 27

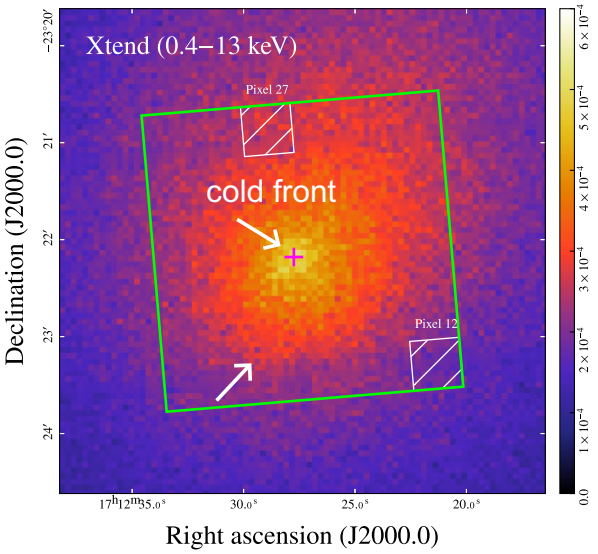

Fig. 1. XRISM Xtend image (0.4–13 keV) of the Ophiuchus cluster overlaid with the Resolve FOV (green box). The magenta cross indicates the X-ray peak. White arrows indicate cold fronts. The positions of pixels 12 and 27 are shown.

Direct measurements of gas velocities in the ICM offer a unique window into these heating processes. High-resolution X-ray spectroscopy can detect both bulk motions (through Doppler shifts of emission lines) and turbulent velocities (through line broadening). Until recently, such measurements were extremely challenging due to the limited spectral resolution of CCD detectors on missions such as Chandra, XMM–Newton, and Suzaku.

The situation changed dramatically with the launch of the Hitomi satellite in 2016, which carried a microcalorimeter capable of achieving spectral resolution of ∼5 eV (Hitomi Collaboration 2016). Although the satellite was short-lived, Hitomi's observations of the cool core of the Perseus cluster provided the direct measurement of ICM turbulence, revealing surprisingly low velocity dispersions of ∼160 km s^{-1} and non-thermal pressure support of only ∼4% (Hitomi Collaboration 2016, 2018a). The observational results of the XRISM satellite (Tashiro et al. 2025), which is the recovery mission of Hitomi, have recently been reported. The velocity dispersions of the cool cores of the Centaurus, Abell 2029, and Hydra A clusters are only ∼120–170 km s^{-1} (XRISM Collaboration 2025a, 2025c; Rose et al. 2025). Even for the Coma cluster, which is a merging cluster, the dispersion is ∼200 km s^{-1} (XRISM Collaboration 2025b).

The Ophiuchus cluster is a nearby galaxy cluster ($z = 0.0296$; Durret et al. 2015) that possesses a cool core despite being a high-temperature cluster ($kT \sim 9$ keV; Fujita et al. 2008). Previous Chandra observations have detected multiple cold fronts and dynamical disturbances within the cool core, suggesting some form of gas motion (Werner et al. 2016; see also figure 1). Radio observations have also reported evidence of past AGN activity of unprecedented scale ($\sim 5 \times 10^{61}$ erg) at the cluster's center (Giacintucci et al. 2020). In this paper, we present the results of our XRISM observations of the Ophiuchus cluster. Our focus is on the velocity structure of the cool core. Other topics, such as metal abundance patterns, will be explored in future work. The cosmological parameters we adopted are $\Omega_0 = 0.3$, $\Lambda = 0.7$, and $h = 0.7$. Thus, 1′ corresponds to 35.6 kpc at the redshift of the Ophiuchus cluster ($z = 0.0296$). The BCG, or central galaxy of the cluster, is 2MASX J17122774−2322108, with a redshift of $z = 0.0295$ (Durret et al. 2015). We use the proto-solar abundance table from Lodders, Palme, and Gail 2009. The quoted errors represent the 1σ statistical uncertainties, unless otherwise mentioned.

2 Observations and data reduction

XRISM observed the central region of the Ophiuchus cluster from 2025 March 31 to April 6 (obsid 201006010), with the aim-point positioned at $\alpha = 258.^{\circ}115$, $\delta = -23.^{\circ}3687$ at the cluster's X-ray center (figure 1). In this paper, we focus on data from the Resolve instrument, a microcalorimeter array that covers a 3.1 × 3.1 arcmin^2 field of view (FOV) with a 6 × 6 pixels configuration (Ishisaki et al. 2022). Each pixel produces a spectrum of incident X-rays with a resolution of 4.5 eV FWHM. The instrument's energy band spans 1.7–12 keV. At low energies, it is limited by the attenuation of the dewar gate valve, which is currently closed. The Resolve data were processed with the latest version 3 software (PROCVER = 03.00.013.010) and analyzed using XRISM FTOOLS wrapped in HEASoft version 6.34 and calibration database (CALDB) version 11. Following the standard screening procedures outlined in the XRISM Data Reduction Guide,[1] the observation yielded a cleaned exposure time of 217 ks.

Each spectrum was obtained by integrating the high-resolution (Hp) grade events across all pixels in the Resolve FOV. We generated spectral redistribution matrix files (RMFs) using the `rslmkrmf` task with "L" size option. The ARF files calculate the effective area by incorporating detector efficiencies and the response of the X-ray Mirror Assembly (XMA), including point spread function (PSF) effects. These files were generated by `xaarfgen` task using the X-ray image from the Chandra satellite as the input brightness distribution. The barycentric correction of 28 km s^{-1} is applied to X-ray velocities in this paper.

3 Spectral modeling and analysis

First, we created maps depicting the temperature (kT), metal abundance (Z), velocity dispersion (σ_v), and redshift of the ICM (z) in order to understand its overall properties. We obtained these maps through a pixel-by-pixel spectral analysis of the Resolve data using a thermal model (bapec). Figure 2 shows the results. The temperature is lower and the abundance is higher in the central nine pixels, which are shifted slightly south-east of the X-ray peak (cyan dashed square). We refer to the region inside the square as the "inner region" and the region outside the square as the "outer region." We note that pixel 27 has been identified to show irregular variation of the energy scale during the observation, which is hard to track using the current gain-monitoring procedure. Thus, we exclude this pixel from the subsequent analysis. We also excluded calibration pixel 12 (figure 1).

We performed a detailed spectral analysis for the two regions. Because the PSF of XRISM is relatively large (∼1.′3 for the half-power diameter), a significant number of photons

[1] ⟨https://heasarc.gsfc.nasa.gov/docs/xrism/analysis/index.html⟩.

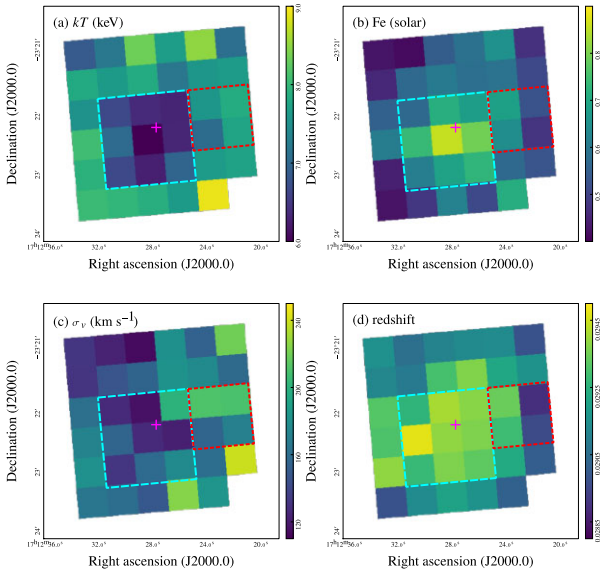

Fig. 2. Maps of (a) temperature, (b) metal abundance, (c) (turbulent) velocity dispersion, and (d) redshift of the ICM obtained with Resolve. The magenta cross shows the X-ray peak, and the cyan dashed square shows the boundary between the inner and outer regions. The red dotted square indicates the area where a peculiar iron line feature was discovered.

emitted from outside a given region may be detected by the telescope as being within the region, and vice versa. We accounted for the spatial-spectral mixing (SSM) effect by fitting the spectra of the two regions simultaneously with plasma models and appropriate weights. Although we took the charged-particle-induced non-X-ray background (NXB) into account, we confirmed that it had little impact on the results. We fit the Resolve spectra with a thermal model (`bapec`) absorbed by photoelectric absorption (`phabs`) using Xspec v12.14.1 (Arnaud 1996) and employed C-statistics (Cash 1979). The Galactic hydrogen column was fixed to the value of $N_{\rm H} = 1.9 \times 10^{21}$ cm^{-2} (HI4PI Collaboration 2016). This study focuses on four key parameters: temperature (kT), abundance (Z), velocity dispersion (σ_v), and bulk velocity ($v_{\rm bulk}$). The latter is estimated from redshift (z) and indicates the systematic velocity relative to the BCG.

Table 1. Best-fitting spectral parameters for the Ophiuchus cluster core.*

Parameter	Inner region ($r \lesssim 25$ kpc)	Outer region ($25 \lesssim r \lesssim 50$ kpc)
kT (keV)	5.8 ± 0.2	8.4 ± 0.2
Z ($Z_\odot$)	0.75 ± 0.03	0.44 ± 0.02
σ_v (km s^{-1})	115 ± 7	186 ± 9
$P_{\rm NT}/P_{\rm tot}$ (%)	1.4 ± 0.2	2.5 ± 0.2
$v_{\rm bulk}$ (km s^{-1})	$+8 \pm 7$	-104 ± 7

*C-stat is 30828.60 with 32562 degrees of freedom.

4 Results

Figure 3a shows the results of fitting the spectra of the two regions simultaneously in the 2–12 keV range, accounting for the SSM effects. Table 1 summarizes the best-fitting parameters. The results do not change within the statistical errors, even when using the 5–12 keV range, because the most prominent lines are Fe lines at ∼6.4–6.8 keV (figures 3b and 3c). As indicated by previous observations (Fujita et al. 2008; Million et al. 2010; Werner et al. 2016), the temperature is lower and the abundance is higher in the inner region compared with the outer region, which is typical for a cool core cluster. The stronger Fe Lyα lines observed in the outer region (figure 3c) reflect a higher temperature than the inner region (figure 3b). The temperature gradient indicates substantial cooling in the

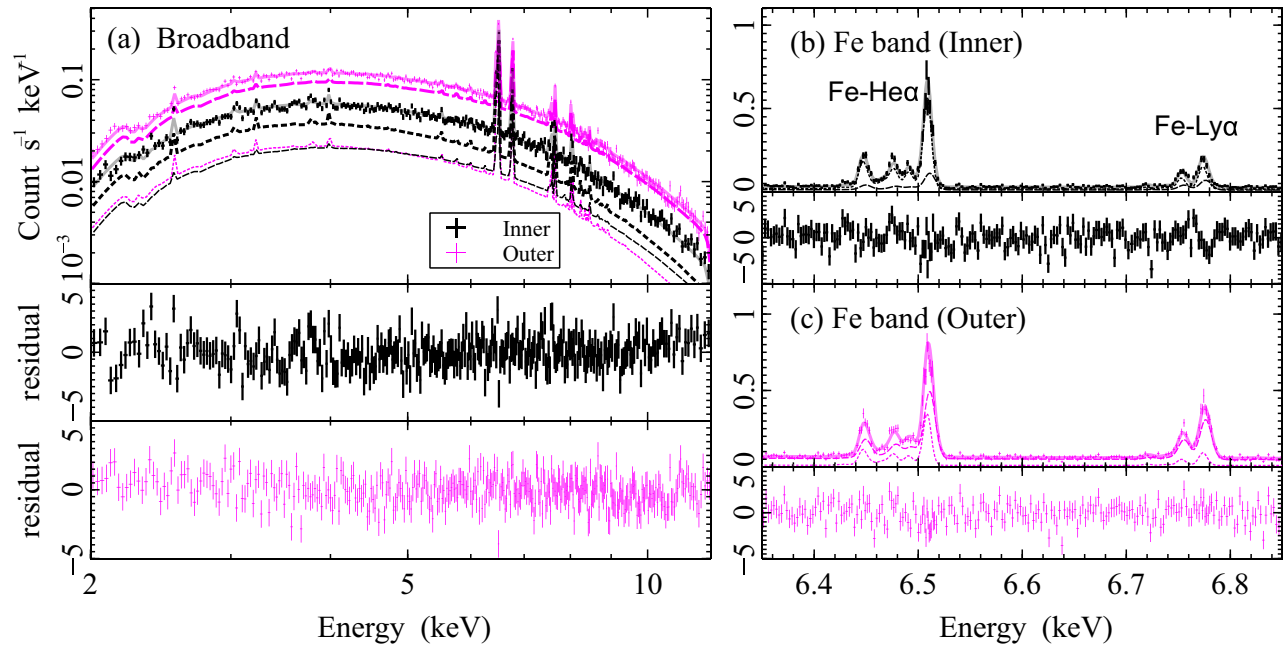

Fig. 3. Resolve spectra and the best-fitting models, including the SSM effect. (a) Broad-band spectra. The black lines show the spectrum of the inner region. From top to bottom, they represent the total spectrum, the inner region's contribution, and the outer region's contribution. The magenta lines show the spectrum of the outer region. From top to bottom, they represent the total spectrum, the outer region's contribution, and the inner region's contribution. (b) and (c) Zoom-in spectra around Fe lines.

central region. The abundance gradient probably reflects the enrichment history of the cluster core, with metals produced by stellar nucleosynthesis in the BCG.

The most significant and surprising result from our XRISM observations is the remarkably low level of gas velocity dispersion in both regions of the Ophiuchus cluster core. The inner region exhibits a velocity dispersion of $\sigma_v = 115 \pm 7\,\mathrm{km\,s^{-1}}$. This is similar to that of the Centaurus cluster ($\sigma_v \lesssim 120\,\mathrm{km\,s^{-1}}$), in which the central AGN activity is weak (XRISM Collaboration 2025c). For the temperature of 5.8 keV, the sound speed is $c_s = 1240\,\mathrm{km\,s^{-1}}$. Assuming that the velocity dispersion determined by Resolve ($\sigma_v = 115\,\mathrm{km\,s^{-1}}$) is entirely due to isotropic turbulence, our measurement implies a turbulent Mach number of $\mathcal{M}_{3D} = \sqrt{3}\sigma_v/c_s = 0.16$, indicating that the motions are highly subsonic. The resulting non-thermal (NT) pressure fraction is

$$\frac{P_{NT}}{P_{tot}} = \frac{\mathcal{M}_{3D}^2}{\mathcal{M}_{3D}^2 + 3/\gamma} = 1.4 \pm 0.2\%, \quad (1)$$

where $\gamma = 5/3$ is the adiabatic index (e.g., Eckert et al. 2019). This value is smaller than those for the central region of the Centaurus cluster ($3.3 \pm 0.6\%$; XRISM Collaboration 2025c) and Abell 2029 ($2.6 \pm 0.3\%$; XRISM Collaboration 2025a); the latter is one of the most dynamically relaxed clusters. It is also significantly smaller than the values for clusters with powerful AGNs, such as Perseus ($3.9 \pm 0.8\%$; Hitomi Collaboration 2016) and Hydra A ($4.5 \pm 0.5\%$; Rose et al. 2025).

For the outer region ($\sigma_v = 186\,\mathrm{km\dot{s}^{-1}}$ and $kT = 8.4$ keV; see table 1), the values are $c_s = 1500\,\mathrm{km\,s^{-1}}$, $\mathcal{M}_{3D} = 0.22$, and $P_{NT}/P_{tot} = 2.5 \pm 0.2\%$. The value of P_{NT}/P_{tot} is still small and comparable to that of Abell 2029. Interestingly, Werner et al. (2016) reported that $\sigma_v \lesssim 100\,\mathrm{km\,s^{-1}}$ based on surface brightness fluctuation analysis. However, they studied the region of $r = 1'.5$–$5'$, most of which is outside the Resolve FOV.

Bulk velocity measurements reveal the relative velocity between the ICM and the BCG. The inner region exhibits an extremely small velocity of $v_{bulk} = +8 \pm 7\,\mathrm{km\,s^{-1}}$. This indicates that the core gas is essentially at rest with respect to the BCG. The Mach number is only $\mathcal{M}_{bulk} = v_{bulk}/c_s = 0.007$. For the outer region, the bulk velocity is $v_{bulk} = -104 \pm 7\,\mathrm{km\,s^{-1}}$ and the Mach number is $M_{bulk} = 0.07$. These bulk velocities are consistent with previous XMM–Newton observations using the EPIC-pn detector, though the velocity uncertainties are significant (Gatuzz et al. 2023).

Considering the steep temperature and abundance gradients at the center of the Ophiuchus cluster (Werner et al. 2016), we conducted a two-component spectral analysis of the inner region, in which kT, σ_v, and v_{bulk} are independent. The abundance Z is common because that of the lower-temperature component cannot be determined. The results are $kT = 2.1^{+0.4}_{-0.2}$ keV, $\sigma_v = 111 \pm 45\,\mathrm{km\,s^{-1}}$, and $v_{bulk} = -41 \pm 48\,\mathrm{km\,s^{-1}}$ for the lower-temperature component, while $kT = 6.5^{+0.3}_{-0.2}$ keV, $\sigma_v = 112 \pm 8\,\mathrm{km\,s^{-1}}$, and $v_{bulk} = +12 \pm 8\,\mathrm{km\,s^{-1}}$ for the higher-temperature component. The abundance is $Z = 0.84 \pm 0.03\,Z_\odot$. The values of σ_v and v_{bulk} for both components are consistent with those of the inner region in table 1. Therefore, it is unlikely that the steep gradients affect the small values of σ_v and $|v_{bulk}|$.

Following previous studies (Churazov et al. 2010; Zhuravleva et al. 2013; Hitomi Collaboration 2018b), we calculated the radial profile of the optical depth of the w resonance line within the He-like Fe α line complex (see figure 4). The line is expected to be most influenced by resonant scattering. In our calculations, we used the ICM density, temperature, and abundance profiles obtained by Werner et al. (2016) and assumed $\sigma_v = 0$. We found that the line is optically thick only in the central few kiloparsec. As the regions we studied are much larger, we expect the influence of resonant scattering to be minimal. In fact, we fit the Resolve spectrum of the inner region by replacing the w resonance line with a Gaussian (zgauss) to include the effect of resonant scattering. We confirmed that the results did not change within the statistical errors.

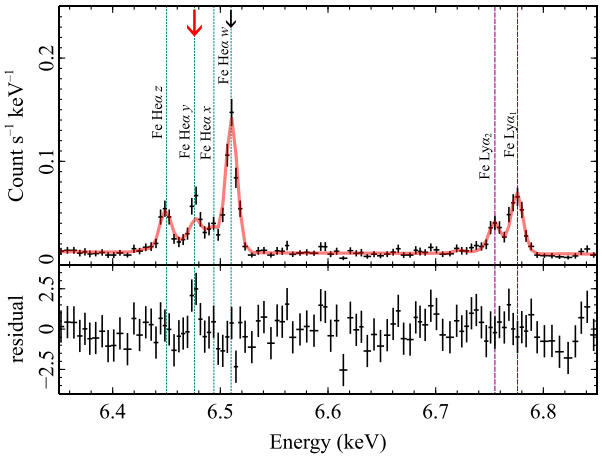

Fig. 4. Spectrum for the west of the cluster center (the region shown by the red dotted square in figure 2). Only the Fe–Heα and Fe–Lyα line complexes are displayed. The red arrow indicates the y intercombination line, and the black arrow indicates the w resonance line within the He-like Fe Kα line complex.

5 Discussion

5.1 Velocity structure

Our XRISM Resolve observations of the Ophiuchus cluster core revealed a quiescent velocity structure. While turbulence could be created by X-ray cavities associated with AGN activity, the extremely low level of turbulence in the inner region ($P_{NT}/P_{tot} = 1.4\%$; table 1) suggests that the central AGN has little kinematic impact on the surrounding ICM. We note that the level of turbulence (1.4%) is nearly the lower limit predicted by TNG-cluster simulations for Perseus-like clusters ($\gtrsim$2%; see figure 4 in Truong et al. 2024).

Turbulence dissipation is expected to heat the gas (Zhuravleva et al. 2014). The turbulent heating rate of gas with a mass density ρ is $Q_{turb} \sim 5\,\rho\sigma_v^3/l_t$, where l_t is the length-scale (Zhuravleva et al. 2014). The radiative cooling rate of the gas is calculated from the gas density and temperature T: $Q_{cool} = n_e n_i \Lambda_n(T)$, where n_e and n_i are the electron and ion number densities, respectively, and $\Lambda_n(T)$ is the normalized cooling function (Sutherland & Dopita 1993). For the inner region, $\sigma_v \sim 115\,\mathrm{km\,s^{-1}}$, $l_t \sim 25$ kpc (the size of the inner region), the temperature $kT \sim 5.8$ keV, and the metal abundance $Z \sim 0.75$ solar, while ρ, n_e, and n_i are obtained from previous Chandra observations ($n_e \sim 0.03\,\mathrm{cm^{-3}}$; Werner et al. 2016). From these values, we obtain $Q_{turb}/Q_{cool} \sim 0.4$, though Q_{turb} depends on the assumption of l_t. This value suggests that turbulent heating could not be ignored in order to counteract radiative cooling. The small

value of $Q_{\rm turb}/Q_{\rm cool} < 1$ is consistent with the absence of observable X-ray cavities in the core and the presence of only weak, point-like radio emission without lobes or jets (Werner et al. 2016). Chandra observations have revealed steep temperature and abundance gradients in the cluster core. These gradients suggest that radiative cooling is ongoing and largely unaffected by AGN heating (Million et al. 2010; Werner et al. 2016). In other words, new powerful AGN activity has not yet been triggered, which suggests that cooling and heating may currently be imbalanced. Another possibility is that other heating mechanisms are at work, such as cosmic-ray streaming (Loewenstein et al. 1991; Guo & Oh 2008; Fujita et al. 2013; Jacob & Pfrommer 2017; Ruszkowski et al. 2017) or thermal conduction (Takahara & Takahara 1979; Narayan & Medvedev 2001).

Cold fronts are contact discontinuities in the ICM and are often considered a sign of bulk motion of the ICM (Markevitch et al. 2000, 2001; Vikhlinin et al. 2001). In the case of the Centaurus cluster, which has multiple cold fronts in its core, oscillating gas motion, or "sloshing," has caused relative motion ($|v_{\rm bulk}| \sim 130$–$310\,{\rm km\,s^{-1}}$) between the ICM and the BCG (XRISM Collaboration 2025c). In contrast, despite the presence of multiple cold fronts, the absolute bulk velocity of the ICM in the cool core of the Ophiucchus cluster is very small ($|v_{\rm bulk}| \lesssim 100\,{\rm km\,s^{-1}}$; table 1). Durret et al. (2015) indicated that the line-of-sight velocity of the BCG is consistent with the mean cluster velocity within the errors, with a difference of $\Delta v = 47 \pm 97\,{\rm km\,s^{-1}}$. These facts could be explained if the inner core, including the BCG, were at rest at the bottom of the cluster's gravitational potential well. However, the sloshing motion of the ICM, induced by past cluster mergers, produced the cold fronts (Fujita et al. 2004) and weakened the AGN activity by shifting the gas accretion center (Million et al. 2010; Hamer et al. 2012; Werner et al. 2016). The sloshing motion may now be approaching a turning point at which the velocity is minimum. The velocity dispersion ($\sigma_{\rm v}$) and the absolute bulk velocity ($|v_{\rm bulk}|$) are both larger in the outer region than in the inner region (table 1). This may be a remnant of the interaction between the core and the surrounding ICM. Another possibility is that the BCG and the associated hot gas are moving almost exactly along the plane of the sky.

5.2 Peculiiar iron line features

XRISM has revealed that ICM spectra often exhibit features that cannot be explained by known physics, such as resonance scattering. For example, the observed flux of the *y* intercombination line within the He-like Fe Kα line complex for Abell 2029 is considerably higher than predicted by the standard collisional ionization equilibrium model (XRISM Collaboration 2025a). An apparent excess of the Fe Lyα_2 line flux over the model has been observed in the Coma cluster (XRISM Collaboration 2025b).

Motivated by the previous studies, we investigated the ICM spectra from 2×2 pixels across the Resolve FOV and found an abnormal feature in the region indicated by the red dotted square in figure 2. Figure 4 shows an excess of the *y* intercombination line, as found in Abell 2029. However, this specific region in figure 2 does not appear particularly unusual, and the origin of the excess is unknown at this time. Such an anomaly will be examined in greater detail using several XRISM observations of other galaxy clusters. Furthermore, laboratory plasma spectroscopy using electron beam ion traps, for instance, will expand our fundamental understanding of atomic physics and emission processes. These findings highlight the importance of collaborative efforts with the atomic physics communities in the XRISM era.

6 Conclusion

Our high-resolution X-ray spectroscopic observations of the Ophiuchus cluster core, conducted with the XRISM satellite, have provided valuable insights into the dynamical state of this system. Despite the presence of previously identified cold fronts and dynamical disturbances, our measurements show that the ICM is remarkably quiescent in the core.

The key findings of this study include the detection of low gas velocity dispersions of $\sigma_{\rm v} = 115 \pm 7\,{\rm km\,s^{-1}}$ in the inner region ($\lesssim$25 kpc) and $186 \pm 9\,{\rm km\,s^{-1}}$ in the outer region (∼25–50 kpc) of the core. These measurements correspond to exceptionally low non-thermal pressure fractions of $1.4 \pm 0.2\%$ and $2.5 \pm 0.2\%$, respectively, indicating that the turbulent motions are highly subsonic. The gas in the inner region is nearly at rest relative to the central galaxy ($|v_{\rm bulk}| = 8 \pm 7\,{\rm km\,s^{-1}}$), while the outer region exhibits moderate motion ($|v_{\rm bulk}| = 104 \pm 7\,{\rm km\,s^{-1}}$). The gas temperatures are $kT = 5.8 \pm 0.2$ keV in the inner region and 8.4 ± 0.2 keV in the outer region, and the metal abundances are $Z = 0.75 \pm 0.03\,Z_\odot$ in the inner region and $0.44 \pm 0.02\,Z_\odot$ in the outer region. These gradients indicate that this is a cool-core cluster.

Using the measured velocity dispersion, we estimate that the turbulent heating rate is only ∼40% of the radiative cooling rate ($Q_{\rm turb}/Q_{\rm cool} \sim 0.4$), although there is some uncertainty. This energy deficit suggests that turbulent heating is currently unable to maintain thermal equilibrium in the cool core, and is consistent with the absence of observable X-ray cavities and the presence of only weak, point-like radio emission without extended lobes or jets. The current thermal imbalance suggests that the cluster may be in a transitional phase in which AGN activity has weakened and cooling has dominated. This indicates that clusters may undergo cyclical phases of heating and cooling imbalance.

Unlike the Centaurus cluster, where cold fronts are associated with significant sloshing gas motion ($|v_{\rm bulk}| \sim 130$–$310\,{\rm km\,s^{-1}}$), the Ophiuchus cluster exhibits cold fronts despite very low bulk velocities. This suggests that the sloshing motion responsible for creating these cold fronts may be approaching a turning point at which the velocity reaches its minimum. This sloshing motion may also have contributed to the weakening of AGN activity by displacing the gas accretion center. Alternatively, the BCG and the associated hot gas could be moving nearly parallel to the plane of the sky.

Our spectroscopic analysis revealed intriguing anomalous features in the Fe line complex. We identified an excess of the *y* intercombination line within the He-like Fe Kα complex in a specific region. This phenomenon is similar to that observed in Abell 2029; however, the origin of this excess remains unclear.

Funding

This work was supported JSPS KAKENHI grant Nos. 22H00158, 23H04899, and 25H00672 (Y. Fujita).

Acknowledgments

We would like to thank the anonymous referee for their useful comments. The authors would also like to thank Kazunori Suda for his estimation of the resonant scattering and Yoshiaki Kanemaru for generating the Xtend image. The authors thank Norbert Werner and John ZuHone for their helpful discussions.

References

Arnaud, K. A. 1996, in ASP Conf. Ser., 101, Astronomical Data Analysis Software and Systems V, ed. H. Jacoby & J. Barnes (San Francisco: ASP), 17
Cash, W. 1979, ApJ, 228, 939
Churazov, E., Brüggen, M., Kaiser, C. R., Böhringer, H., & Forman, W. 2001, ApJ, 554, 261
Churazov, E., Forman, W., Jones, C., & Böhringer, H. 2000, A&A, 356, 788
Churazov, E., Zhuravleva, I., Sazonov, S., & Sunyaev, R. 2010, Space Sci. Rev., 157, 193
Durret, F., Wakamatsu, K., Nagayama, T., Adami, C., & Biviano, A. 2015, A&A, 583, A124
Eckert, D., et al. 2019, A&A, 621, A40
Fabian, A. C. 1994, ARA&A, 32, 277
Fabian, A. C. 2012, ARA&A, 50, 455
Fujita, Y., et al. 2008, PASJ, 60, 1133
Fujita, Y., Kimura, S., & Ohira, Y. 2013, MNRAS, 432, 1434
Fujita, Y., Matsumoto, T., & Wada, K. 2004, ApJ, 612, L9
Fujita, Y., & Ohira, Y. 2013, MNRAS, 428, 599
Gatuzz, E., et al. 2023, MNRAS, 522, 2325
Giacintucci, S., Markevitch, M., Johnston-Hollitt, M., Wik, D. R., Wang, Q. H. S., & Clarke, T. E. 2020, ApJ, 891, 1
Guo, F., & Oh, S. P. 2008, MNRAS, 384, 251
Hamer, S. L., Edge, A. C., Swinbank, A. M., Wilman, R. J., Russell, H. R., Fabian, A. C., Sanders, J. S., & Salomé, P. 2012, MNRAS, 421, 3409
HI4PI Collaboration 2016, A&A, 594, A116
Hillel, S., & Soker, N. 2017, MNRAS, 466, L39
Hitomi Collaboration 2016, Nature, 535, 117
Hitomi Collaboration 2018a, PASJ, 70, 9
Hitomi Collaboration 2018b, PASJ, 70, 10
Ikebe, Y., et al. 1997, ApJ, 481, 660
Ishisaki, Y., et al. 2022, in Proc. SPIE, 12181, Space Telescopes and Instrumentation 2022: Ultraviolet to Gamma Ray, ed. J.-W. A. den Herder et al. (Bellingham, WA: SPIE), 121811S
Jacob, S., & Pfrommer, C. 2017, MNRAS, 467, 1478
Kaastra, J. S., Ferrigno, C., Tamura, T., Paerels, F. B. S., Peterson, J. R., & Mittaz, J. P. D. 2001, A&A, 365, L99
Kravtsov, A. V., & Borgani, S. 2012, ARA&A, 50, 353
Lodders, K., Palme, H., & Gail, H.-P. 2009, Landolt Börnstein, 4B, 712
Loewenstein, M., Zweibel, E. G., & Begelman, M. C. 1991, ApJ, 377, 392
Markevitch, M., et al. 2000, ApJ, 541, 542
Markevitch, M., Vikhlinin, A., & Mazzotta, P. 2001, ApJ, 562, L153
McNamara, B. R., & Nulsen, P. E. J. 2007, ARA&A, 45, 117
Million, E. T., Allen, S. W., Werner, N., & Taylor, G. B. 2010, MNRAS, 405, 1624
Narayan, R., & Medvedev, M. V. 2001, ApJ, 562, L129
Peterson, J. R., et al. 2001, A&A, 365, L104
Rose, T., et al. 2025, ApJ, 990, 42
Ruszkowski, M., Yang, H.-Y. K., & Reynolds, C. S. 2017, ApJ, 844, 13
Sarazin, C. L. 1988, X-Ray Emission from Clusters of Galaxies (Cambridge: Cambridge University Press)
Sutherland, R. S., & Dopita, M. A. 1993, ApJS, 88, 253
Takahara, M., & Takahara, F. 1979, Prog. Theor. Phys., 62, 1253
Tamura, T., et al. 2001, A&A, 365, L87
Tashiro, M., et al. 2025, PASJ, 77, S1
Truong, N., Pillepich, A., Nelson, D., Zhuravleva, I., Lee, W., Ayromlou, M., & Lehle, K. 2024, A&A, 686, A200
Vikhlinin, A., Markevitch, M., & Murray, S. S. 2001, ApJ, 551, 160
Werner, N., et al. 2016, MNRAS, 460, 2752
XRISM Collaboration 2025a, ApJ, 982, L5
XRISM Collaboration 2025b, ApJ, 985, L20
XRISM Collaboration 2025c, Nature, 638, 365
Zhuravleva, I., et al. 2014, Nature, 515, 85
Zhuravleva, I., et al. 2013, MNRAS, 435, 3111

Received: 2025 July 1; Accepted: 2025 July 27